CORE
Metadata, citation and similar papers at core.ac.uk
Provided by CERN Document Server

Hyperfine Interactions 129 (2000) 461–473

Electron–gamma perturbed angular correlation studies on high-T_C superconductors

J.G. Correia [a,b], J.P. Araújo [c], J.G. Marques [a,d], A.R. Ramos [a], A.A. Lourenço [e], V. Amaral [e], V. Galindo [f], J.P. Senateur [f], F. Weiss [f], U. Wahl [g], A.A. Melo [a], J.C. Soares [a,d], J.B. Sousa [c] and the ISOLDE collaboration [b]

[a] *CFN, University of Lisboa, Av. Prof. Gama Pinto 2, P-1699 Lisboa Codex, Portugal*
[b] *EP/SC Division, CERN, CH-1211 Geneva, Switzerland*
[c] *IFIMUP, University of Porto, Rua do Campo Alegre 687, P-4150 Porto, Portugal*
[d] *ITN, Estrada Nacional 10, P-2685 Sacavém, Portugal*
[e] *Physics Department, University of Aveiro, P-3800 Aveiro, Portugal*
[f] *UMR CNRS 5628, INPG-ENSPG, BP 46, F-38402 St. Martin D'Hères Cedex, France*
[g] *IKS, University of Leuven, Celestijnenlaan 200 D, B-3001 Leuven, Belgium*

Recent results on the study of high-T_C superconductors using the $e^- - \gamma$ perturbed angular correlation technique are presented. The basic features of the experimental equipment and its installation at the ISOLDE facility are briefly described. Results obtained from ^{197m}Hg implanted into high quality $Y_1Ba_2Cu_3O_{6+\delta}$ epitaxy thin films are presented and discussed.

Keywords: nuclear techniques, hyperfine fields, high-T_C superconductors

open-2001-014
01/08/1999

1. Introduction

The discovery of high-T_C superconductors (HTS) triggered an intense experimental and theoretical research program in the last decade. Hundreds of new materials were synthesised and new cuprate families of superconductors with increasing critical temperature were produced [1,2]. However, many problems at the structural microscopic level remained unclear [3–5]. The structure of the cuprates can be described by the intergrowth of two block layers along the crystallographic c-axis, as represented in figure 1, i.e., the superconducting (*Sc*) layer, with an oxygen deficient perovskite-like structure in which n CuO_2 layers alternate with cation layers (M), and the charge reservoir (*CR*) layers which have usually a rocksalt-like structure with two cations A and B. The cations are arranged in two B-O outer planes directly bound to the *Sc* block layers, while m planes of the composition A-O are located in between the B-O planes. In contrast with the *Sc* layers, the *CR* ones have several chemical configurations and behave as insulators or metals, depending on the presence of chemical and/or structural defects. Changes of the oxygen concentration in these blocks can cause metal to insulator transitions and structural changes, and will induce an injection of charge carriers in the superconducting blocks.

© J.C. Baltzer AG, Science Publishers

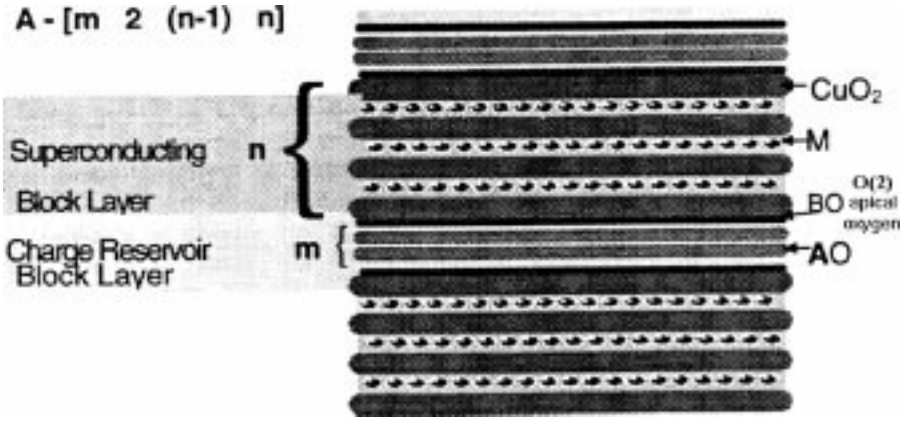

Figure 1. Schematic representation of the cuprate structure of the high-TC superconductors, from [4].

The understanding of the mechanisms that regulate the transfer of charge carriers between the *CR* and the *Sc* blocks is a major point of present experimental research [5,6]. In particular, the replacement of elements in the *CR* block layer by elements or chemical groups with different oxidation states is of special interest since it is expected that such doping induces changes of the HTS properties [7]. However, the number of impurities, which can be incorporated during growth, limits the amount of replacements. Furthermore, the common techniques,[1] which are used to characterise the new *CR* structures, are often not able to characterise on an atomic scale the order/disorder and their interactions with point defects of both the lattice constituent and the dopant elements.

The specific advantages of nuclear spectroscopic techniques, which use radioactive isotopes to study HTS are still far from being exploited. Previous studies using Mössbauer Spectroscopy [8], Perturbed Angular Correlations (PAC) [9] and Emission Channeling (EC) [10] were limited by the small number of suitable probe elements and by the poor quality of the available samples of superconductors.

An interdisciplinary collaboration received an approved proposal at ISOLDE/CERN [11] for research in high-T_C Superconductors [3]. The work of this collaboration has been recently summarised in [12,13]. From that work, examples of the application of $e^- - \gamma$ PAC technique to studies of the Hg doping of $YBa_2Cu_3O_{6+x}$ (YBCO) high quality thin films will be shown.

2. Experimental details

The PAC technique has demonstrated its potential when applied to systems as diverse as metals, semiconductors, insulators and biological molecules [14,15]. Being highly sensitive to the probe's atomic neighbourhood, PAC measures the electric field

[1] E.g., electron microscopy, Raman and infra-red spectroscopy, synchrotron radiation and X-ray analysis, neutron diffraction and iodometry (for determination of oxygen content).

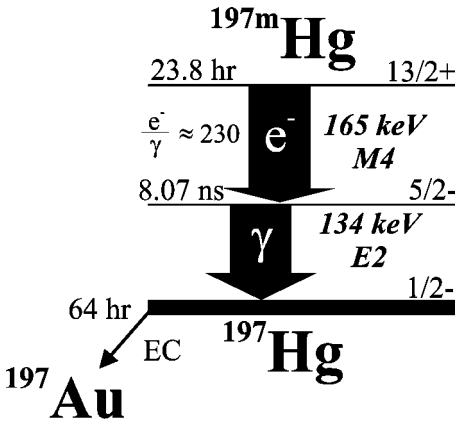

Figure 2. Schematic representation of the decay of ^{197m}Hg.

gradient (EFG) which is generated by the deviation from cubic symmetry of the charge distribution around the probe nuclei [16]. However, the number of suitable radioactive isotopes is limited. In many cases γ–γ cascades can be substituted with advantage by e^-–γ cascades, enlarging the number and variety of PAC probes. Such is the case for, e.g., ^{73}As [17], ^{127}Ba [18], ^{119m}Sn and ^{197m}Hg, where at least one of the transitions is highly converted. In these extreme cases γ–γ experiments are just not feasible. Furthermore, a larger experimental anisotropy is normally obtained, due to a favourable electron particle parameter.

At ISOLDE the ^{197m}Hg nuclei are produced by bombardment of a molten Pb target with the 1 GeV proton beam from the PS-Booster accelerator at CERN [11]. ^{197m}Hg has a 24 h half-life and decays via a 165–134 keV cascade, shown in figure 2. Both the K and L-conversion electrons from the 165 keV transition can be selected. Figure 3 shows a conversion electron spectrum obtained in the decay of ^{197m}Hg. The L-conversion electrons are more convenient due to a higher conversion ratio and higher energy, which improves the time resolution. ^{197}Hg then decays to ^{197}Au with 64 h half-life. The quadrupole moment of the 134 keV state in ^{197}Hg has been recently re-evaluated to be $Q(^{197}\text{Hg}) = -0.057 \pm 0.007$ b [19].

The e^-–γ PAC spectrometer consists of two magnetic lenses of the Siegbahn type [20] for detection of conversion electrons, and two BaF_2 scintillators for γ detection, all arranged in one plane. As shown in figure 4, each lens is at relatively 90° with one γ detector and 180° with the other. In this way a classical four-detector PAC spectrometer is formed, with two start-detectors and two stop-detectors. The sample is situated inside a vacuum chamber, with the side to be implanted facing both magnetic lenses.

For on-line implantation and measurement, the ISOLDE ion beam enters the chamber through a narrow tube, 30 cm long and 1.2 cm wide, mounted in between the magnetic lenses. Albeit this narrow aperture, a beam transmission of 90% is achieved. The sample holder is mounted on a feed-through system that allows sample changing

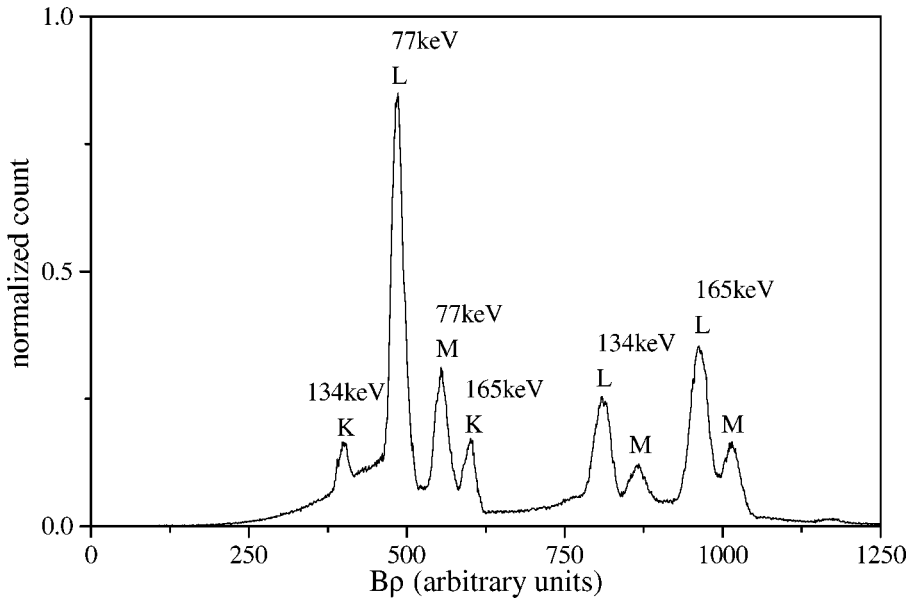

Figure 3. Electron spectrum from the decay of ^{197m}Hg and ^{197}Hg. The spectrum shows already a strong concentration of nuclei in the ^{197}Hg ground state, which is revealed by the intense L and M 77 keV conversion lines from the decay of ^{197}Hg to ^{197}Au. Legend: $B\rho = p/e$, where $B =$ magnetic field, $\rho =$ curvature radius of the focusing trajectory in the magnetic spectrometer, $p =$ electron momentum and $e =$ electron charge.

without breaking the vacuum in the chamber. Moreover, by having the sample holder directly connected to heating equipment, it is possible to implant and measure within a large temperature range. Measurements can also be performed off-line, e.g., when complex annealing procedures are required. When performing e^-–γ PAC experiments at low temperatures it is essential to avoid the condensation of residual gas at the sample's surface, since that will absorb and scatter the conversion electrons emitted by the shallow implanted radioactive nuclei. Absorption and scattering lead to a decrease of the electron intensity, to the electron energy spread and, most important, to the loss of the anisotropy of the angular correlation, in particular for low energy electrons. With the successful installation of a cryogenic system, which allows cooling of the samples down to 30 K, low temperature e^-–γ PAC experiments will soon become feasible [21]. Under typical working vacuum of $\sim 5 \times 10^{-7}$ mbar, the condensation of residual gas at the sample's surface was efficiently reduced. Therefore the experiments can run at 30 K during 48 h periods after which the sample's surface should be baked, to remove the condensed gas, by heating it up to RT.

A magnetic lens has specific advantages for PAC studies. Compared to the usual NaI or BaF_2 scintillators used in γ–γ PAC, the energy resolution of the electron detector is better, usually in the order of a few percent, and the conversion electrons from the right transition can be selected without admixtures from other ones. Since energy selection takes place before detection, the count rate in the detector is sig-

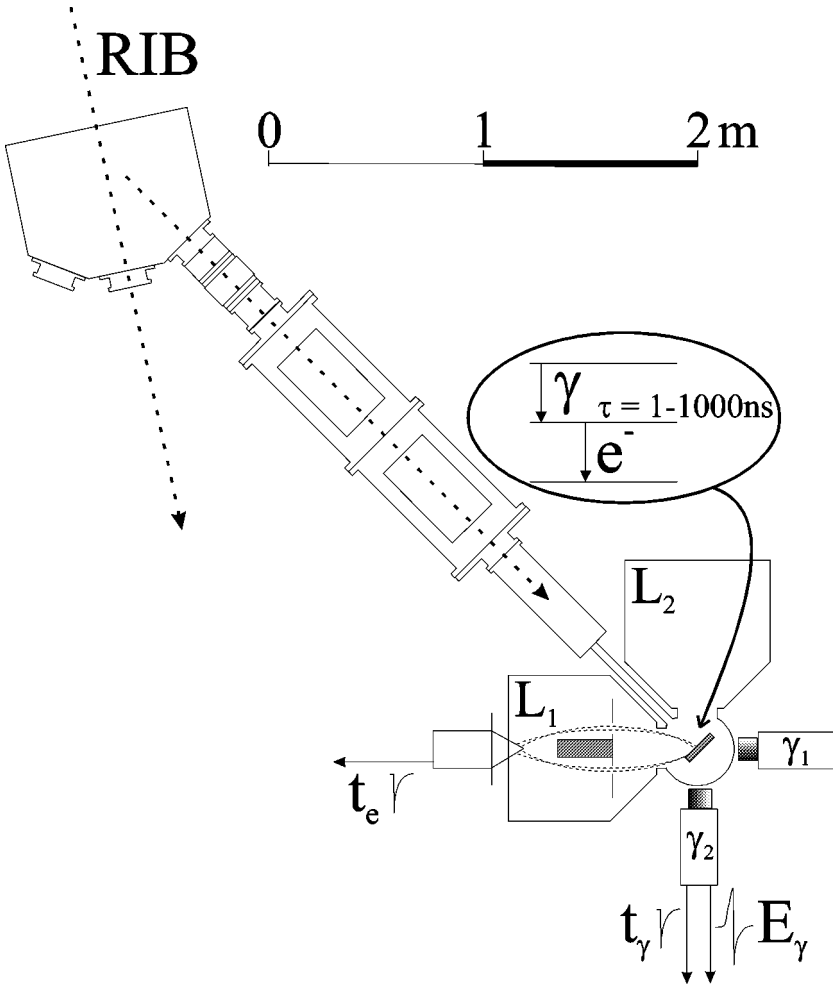

Figure 4. General view of the γ–e^- PAC spectrometer mounted on-line with the ISOLDE beam line [18]. Legend: RIB = radioactive ion beams; L_1, L_2 = electron magnetic lens 1 and lens 2; t_e, t_γ = anode signals used for time analysis from the electron and gamma photomultipliers, respectively; E_γ = dynode signal used for γ-ray energy discrimination.

nificantly reduced. In this way it is possible to use weak lines in the presence of other intense transitions, or to use stronger activities without overloading the detectors and subsequent electronic circuits. Electron detection in the magnetic lenses is achieved using plastic scintillators in order to optimise the time resolution. The energy resolution of the plastic scintillators is only important for low energy electrons ($E < 15$ keV), for which most of the signal falls within the photomultiplier's noise. To separate efficiently the signal for such low energy electrons a pre-acceleration system has been developed and successfully used in several measurements with the ^{73}Ge probe [17].

The currently used BaF_2 scintillators are 2″ thick to ensure a good efficiency for a wide range of energies. Transistorised bases coupled to XP2020Q photomultipliers ensure a stable operation up to 200 kHz for anode pulses with about −1000 mV amplitude. The time resolution for the e^-–γ ^{197m}Hg cascade is 1 ns (FWHM).

The PAC spectrometer collects 4 time spectra from time coincidences between the conversion electron and the gamma radiation from the first and the second transitions. These are detected by one electron-gamma detector pairs at relative angles of $\theta = 180°$ or $\theta = 90°$, whose counting rates are denoted by $N_j(180°, t)$ and $N_i(90°, t)$, $j = i = 1, 2$, respectively. The experimental function $R(t)$ is constructed according to eq. (1).

$$R(t) = 2\frac{\sqrt{\prod_j^2 N_j(180°, t)} - \sqrt{\prod_i^2 N_i(90°, t)}}{\sqrt{\prod_j^2 N_j(180°, t)} + 2\sqrt{\prod_i^2 N_i(90°, t)}}. \tag{1}$$

This ratio eliminates the half-life exponential component, revealing the perturbation function that contains all the relevant information. For each angle θ the angular correlation functions $W(\theta, t)$ are calculated numerically when the EFGs are oriented (in single-crystalline samples) or randomly distributed (in poly-crystalline samples), by taking into account the full Hamiltonian for the quadrupole hyperfine interaction [16,22]. Equation (2) defines the theoretical function, $R_{\text{fit}}(t)$, whose parameters are fitted to the experimental function $R(t)$.

$$R_{\text{fit}}(t) = 2\frac{W(180°, t) - W(90°, t)}{W(180°, t) + 2W(90°, t)}. \tag{2}$$

For a cascade with an intermediate level with spin $I = 5/2$, three frequencies are observable per EFG. From these frequencies the coupling constant of the interaction, $\nu_Q = eQV_{zz}/\text{h}$, and the asymmetry parameter $\eta = (V_{xx} - V_{yy})/V_{zz}$ can be extracted. V_{zz} is the principal component of the EFG tensor that is produced by the charge distribution outside the probe nucleus and Q is the quadrupole moment of the 134 keV excited state.

In the case of an interaction with randomly distributed defects, a distribution of frequencies is observed instead of a sharp frequency. In this work the EFG distributions are only due to the implantation defects. Then, before annealing, we assume static EFG interactions and represent them with a Gaussian-like distribution that is characterised by a mean value $\langle\nu_Q\rangle$ and standard deviation σ_Q [23]. $\langle\nu_Q\rangle$ and σ_Q depend on the density and variety of the lattice defects.

3. Experimental results

The YBCO compound is one of the most studied and interesting HTS materials for applications. Doping studies have shown that the YBCO T_C is always lowered except for doping with Au or Hg which increases T_C by 2 K [24] and 10 K [25], respectively. In [25] Hg was introduced into YBCO during sintering by changing the

composition of the reactants. By replacing a few percent of Ba by Hg it was expected to dope the YBCO charge carrier block reservoirs. However, in those works the Hg site was not measured, and the presence of several crystalline phases, other than YBCO, cannot be excluded.

In the present work radioactive ^{197m}Hg was implanted into YBCO thin films by 60 keV ion implantation at a low dose of 1×10^{13} at. cm^{-2}, thus, avoiding amorphization and the formation of different crystalline phases. The crystalline quality and T_C have been controlled in the as-grown state and also after the implantation and subsequent annealing treatments. For this purpose the Rutherford backscattering/channeling technique and the measurement of T_C with the alternate susceptibility (χ_{ac}) technique have been used [26–28].

Figure 5(a) shows a PAC spectrum measured on a single-crystalline-like film at room temperature (RT) after ^{197m}Hg implantation and subsequent annealing the sample at 723 K in flowing O_2. The film was placed with its normal ($\vec{n}$) in the detector's plane, under an angle of 45° to each electron detector. X-ray diffraction showed that the film was epitaxially grown, with the c-axis pointing towards $\vec{n}$. The $R(t)$ spectrum was fitted assuming that all Hg probe nuclei interact with the same EFG$_1$, characterised by a sharp ($\sigma_{Q1} = 0$) frequency centred at $\langle \nu_{Q1} \rangle = 121.5 \pm 0.4$ MHz, where V^1_{zz} is aligned along c, and a small $\eta = 0.19 \pm 0.02$. The value $\sigma_{Q1} = 0$ reflects the fact that no point defects remain in the Hg atomic vicinity. Figures 5(b) and (c) show refined measurements of the EFG orientation where $R(t)$ spectra have been measured with $\vec{n}$ placed in the detector plane but now under angles of 18° and 72° with respect to each electron detector directions, respectively. In these pictures the continuous lines are just simulations of the $R(t)$ spectra, assuming that V^1_{zz} is fully aligned with $\vec{n} \parallel c$, but now under an angle of 18° or 72° with respect to the electron detector. The agreement between the experimental data and the simulations is remarkable, thus, confirming that Hg is located at unique sites of the YBCO lattice and surrounded by a charge distribution with the lattice symmetry. The fact that the magnitude of $|V^1_{zz}|$ is very close to $|V_{zz}|$ measured in ^{199m}Hg doped HgO strengthens the supposition that Hg in YBCO has two linear coordinated (apical) oxygen atoms as first neighbours, as it is the case for the Cu(1) lattice site [26]. Complementary EC experiments and EC simulations, which have shown that Hg lies along the Cu c-axis rows, further support this interpretation [29].

Figure 6 shows $R(t)$ spectra measured at several temperatures up to 757 K. The vacuum was kept at 3×10^{-6} mbar [26,27]. All spectra are again fitted with only one main EFG interaction. Below 587 K that is characterised by one frequency triplet that reveals a slightly unsymmetrical but still unique EFG$_1$. The strong attenuation of the as-implanted spectrum, which disappears at 511 K, is due to Hg nuclei that interact with randomly distributed defects. Within the PAC range of sensitivity of a few nanometres around the Hg probe nuclei, the lattice recovers by annealing at 511 K and no point defects remain in the Hg neighbourhood. For annealing temperatures above 511 K EFG$_1$ becomes axially symmetric ($\eta = 0$), thus, revealing that the orthorhombic-to-tetragonal structural transition has occurred in our thin films between 511 and 587 K.

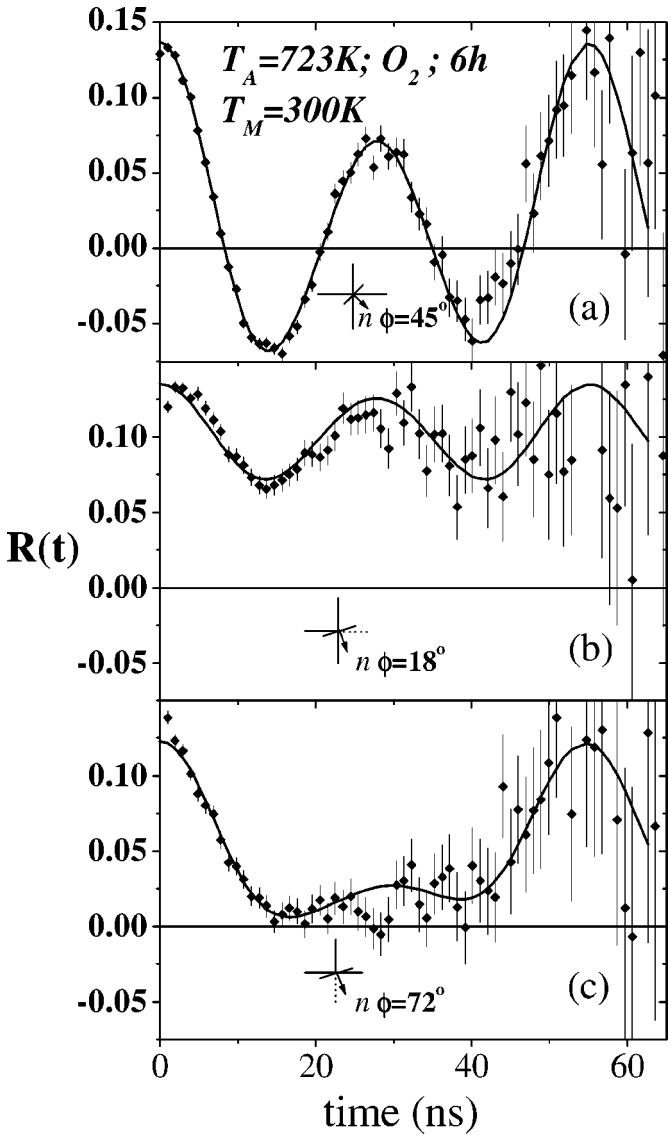

Figure 5. PAC spectra measured on a single-crystalline-like film at RT after implantation and annealing under flowing O_2 at 723 K. (a) $\vec{n}$ is at 45° with both electron detectors; (b)–(c) $\vec{n}$ is at 18° (b) and 72° (c) with each electron detector, respectively, [27].

In agreement with this, the χ_{ac} measurements show that due to the vacuum annealing, the superconductor compound was transformed into an antiferromagnetic insulator. Superconductivity was then reestablished, and T_C recovered to the as-grown value, after 6 h annealing under O_2 flow at 723 K [27].

When annealing in vacuum above 653 K Hg starts to diffuse out of the sample and the $R(t)$ spectra change irreversibly. Above 757 K only EFG_2 is present with

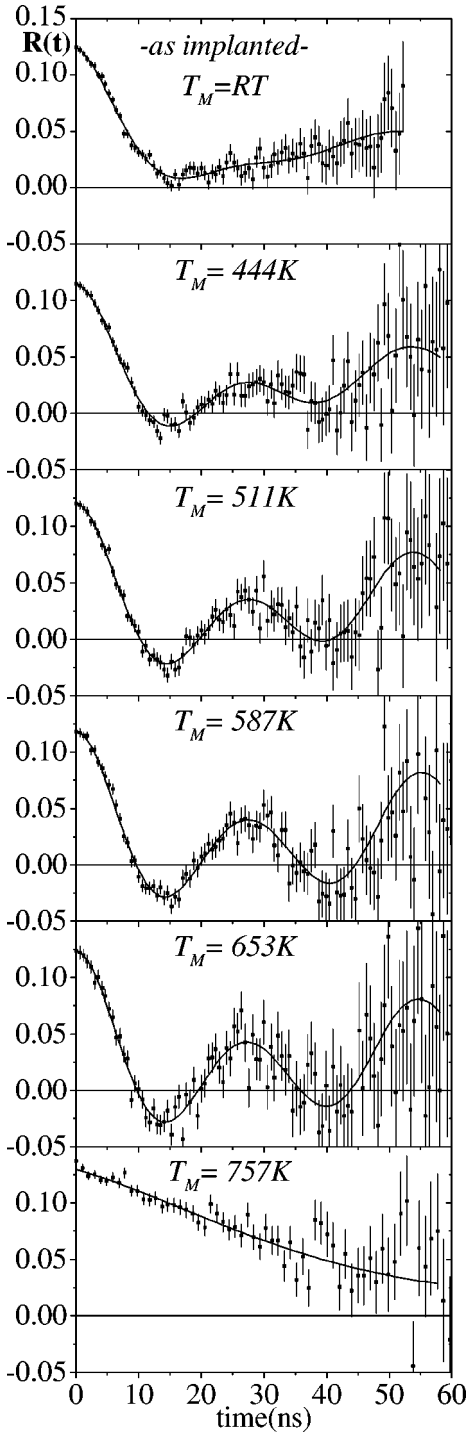

Figure 6. PAC spectra measured after implantation and during annealing in vacuum up to 757 K [26].

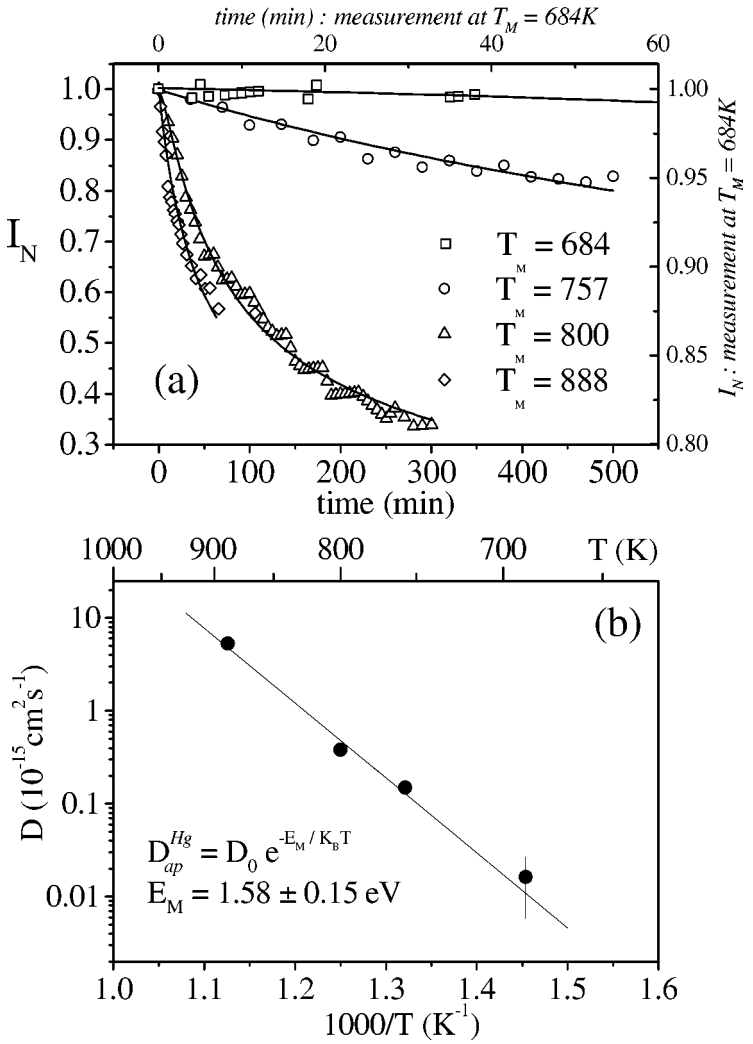

Figure 7. (a) I_N plotted as a function of annealing time (I_N = average of CRγ and CR_{PAC} count rates after half-life correction and normalisation, see text). At 684 K the diffusion is very slow and during a short analysis only few points were taken. For the clearness of the picture, these points are plotted with different scales that are shown at the top and right axis. (b) Arrhenius plot of the apparent Hg diffusion coefficient. Solid lines are fits detailed in [27].

parameters $\langle \nu_{Q2} \rangle = 23 \pm 3$ MHz and $\sigma_{Q2} = 25 \pm 9$ MHz. Moreover, this effect is irreversible when returning to lower annealing temperatures. The fact that $\nu_{Q2} \ll \nu_{Q1}$ is a hint that diffusion of the Hg ions must take place in lattice sites with higher symmetry, most likely not bound to oxygen anymore.

The Hg outdiffusion was studied by measuring as a function of annealing time the γ count rate CR_γ of the 134 keV transition and the PAC coincidence rate CR_{PAC} at constant temperature. At a temperature of 653 K (and higher 684, 757, 800 and

888 K) both CR_γ and CR_{PAC} decrease faster than expected from the ^{197m}Hg decay. When analysing the data, the count rates were corrected for the natural decrease due to the radioactive decay, and normalised to unity at the beginning of each measurement. The decrease of CR_γ and CR_{PAC} with time was equal, thus indicating that Hg is diffusing out. If Hg would only diffuse within the film, then CR_{PAC} would decrease faster than CR_γ, due to higher absorption and scattering of the conversion electrons through the film.

Figure 7(a) shows the average (I_N) of the CR_γ and CR_{PAC} corrected normalised intensities. It is clearly seen that the rate of Hg loss increases with T_M. I_N is proportional to the remaining ^{197m}Hg nuclei in the film, thus it is proportional to the integral in depth of the Hg density distribution. The solid lines in figure 7(a) are fits assuming a simple one-dimension Gaussian-like diffusion distribution in a semi-infinite film without surface traps, as described in detail in [27]. The apparent diffusion coefficient $D_{ap}^{Hg}(T_M)$ obtained is plotted as a function of the reciprocal temperature in figure 7(b). The solid line is a fit with an Arrhenius law from which the migration energy for Hg in oxygen deficient YBCO lattice was found to be $E_M = 1.58 \pm 0.15$ eV. Finally, the abundance of oxygen seems to delay the Hg diffusion, since after annealing at 723 K under O_2 flow only a small amount of Hg was lost and the value of EFG_1 did not change.

4. Conclusions

In this paper applications of the e^-–γ PAC technique to study low concentration Hg doped YBCO at the atomic level were presented and discussed. It was shown that Hg atoms occupy unique lattice sites of the YBCO structure, which are stable up to high annealing temperatures. Under our specific sample preparation conditions, after the implantation and subsequent annealing treatments used in this work, we can exclude that Hg occupies the Ba/Y sites. New Hg-YBCO phases will be further studied where higher Hg doping is achieved by diffusion. The recent cryogenic system for cooling down samples to be measured with the e^-–γ PAC technique will allow for further extended studies on low temperatures.

Acknowledgements

This work was partially funded by FCT, Portugal, through projects CERN/P/FIS/1024/98 and PBICT/C/CTM/1891/95, and grants under the PRAXIS XXI Program (J.P.A., A.R.R.). R. Catherall is further acknowledged for proof reading.

References

[1] J.G. Bednorz and K.A. Müller, Z. Phys. B 64 (1986) 189.
[2] S.N. Putilin, E.V. Antipov, O. Chmaissem and M. Marezio, Nature 362 (1993) 226; A. Schilling, M. Cantoni, J.D. Guo and H.R. Ott, Nature 363 (1993) 56.

[3] J.G. Correia et al., Studies of high-Tc superconductors doped with radioactive isotopes, CERN/ISC 96-30, ISC/P86, IS360 (1996).
[4] M. Lagues et al., in: *Coherence in High Temperature Superconductors*, eds. G. Deutscher and A. Revcolevschi (World Scientific, Singapore, 1996) p. 70.
[5] P. Bordet, F. Duc, P.G. Radaelli, A. Lanzara, N. Saini, A. Bianconi and E.V. Antipov, Phys. C 282–287 (1997) 1081.
[6] J.T. Market, Y. Dalichaouch and M.B. Maple, in: *Physical Properties of High Temperature Superconductors I*, ed. D.M. Ginsberg (World Scientific, Singapore, 1989) p. 265;
C.L. Chien, G. Xiao, M.Z. Cieplak, D. Musser, J.J. Rhyne and J.A. Gotaas, in: *Superconductivity and Its Applications*, eds. H.S. Kwok and D.T. Shaw (Elsevier, New York, 1988) p. 110.
[7] S.M. Loureiro, private communication.
[8] L. Bottyán, B. Molnár, D.L. Nagy, I.S. Szücs, J. Tóth, J. Dengler, G. Ritter and J. Schober, Phys. Rev. B 38 (1988) 11373;
I.S. Lyubutin, V.G. Terziev and A.Ya. Shapiro, Hyp. Interact. 61 (1990) 1105.
[9] P. Singh, M.N. Nyayate, S.H. Devare and H.G. Devare, Phys. Rev. B 39 (1989) 2308;
M. Uhrmacher and A. Bartos, Hyp. Interact. 61 (1990) 1073;
W. Tröger and T. Butz, Z. Naturforsch. 47a (1992) 12.
[10] A. Bartos, H. Plank, D. Forkel, S. Jahn, J. Markel, R. Polewka, M. Uhrmacher, S. Winter, W. Witthuhn and the ISOLDE Collaboration, J. Less-Comm. Metals 164/165 (1990) 1121.
[11] E. Kugler, D. Fiander, B. Jonson, H. Haas, A. Przewloka, H.L. Ravn, D.J. Simon, K. Zimmer and the ISOLDE Collaboration, Nucl. Instrum. Methods B 70 (1992) 41;
B. Jonson, H.L. Ravn, and G. Walter, Nucl. Phys. News 3(2) (1993) 5.
[12] J.G. Correia and the IS360 collaboration [3], CERN Ann. Rep., Vol. II (1997) p. 101; and CERN Ann. Rep., Vol. II (1998).
[13] J.G. Correia and the IS360 collaboration [3];
E. Alves, V.S. Amaral, J.P. Araújo, P. Bordet, T. Butz, J.J. Capponi, B. Ctortecka, S. Le Floch, V. Galindo, R. Gatt, H. Haas, G. Langouche, S.M. Loureiro, A.A. Lourenço, J.G. Marques, A.A. Melo, T. von Papen, A.R. Ramos, J.P. Senateur, M.F. da Silva, J.C. Soares, J.B. Sousa, P. Toulemonde, W. Tröger, A. Vantomme, U. Wahl, F. Weiss and the ISOLDE collaboration, High-Tc Superconductors Studies with Radioactive Ion Beams at ISOLDE, in: *Proc. of OECD/NEA Workshop on Ion and Slow Positron Beams* (September 1998) Costa da Caparica, Portugal (in press).
[14] R. Vianden, Hyp. Interact. 35 (1987) 1079.
[15] A. Lerf and T. Butz, Hyp. Interact. 36 (1987) 275.
[16] Th. Wichert, N. Achziger, H. Metzner and R. Sielemann, in: *Hyperfine Interactions of Defects in Semiconductors*, ed. G. Langouche (Elsevier, Amsterdam, 1992) p. 1.
[17] J.G. Correia, H. Haas, J.G. Marques, A.A. Melo, J.C. Soares and the ISOLDE Collaboration, Hyp. Interact. 80 (1993) 1321.
[18] J.G. Correia, J.G. Marques, J.C. Soares, A.A. Melo, H. Haas and the ISOLDE Collaboration, Nucl. Instrum. Methods B (in press).
[19] W. Tröger, T. Butz, P. Blaha and K. Schwarz, Hyp. Interact. 80 (1993) 1109;
P. Herzog, K. Krien, K. Freitag, M. Reuschenbach and H. Walitzki, Nuclear Phys. A 337 (1980) 261.
[20] J.G. Marques, J.G. Correia, A.A. Melo, M.F. da Silva, J.C. Soares and the ISOLDE Collaboration, Nucl. Instrum. Methods B 99 (1995) 645.
[21] F. Espírito-Santo, J.G. Correia, A.A. Melo, J.P. Araújo, J.G. Marques and J.C. Soares, in preparation.
[22] N.P. Barradas, M. Rots, A.A. Melo and J.C. Soares, Phys. Rev. B 47 (1993) 8763.
[23] M. Deicher, Hyp. Interact. 79 (1993) 681.
[24] G. Ganakas, M.J. Morgan and G. Jakovidis, J. Mater. Sci.: Mater. Electr. 6 (1995) 244.
[25] A.K. Chakraborty, K. Bose, G. Som and B.K. Chaudhuri, J. Mater. Sci.: Mater. Electr. 5 (1994) 22.

[26] J.P. Araújo, J.G. Correia, U. Wahl, J.G. Marques, E. Alves, V.S. Amaral, A.A. Lourenço, V. Galindo, T. von Papen, J.P. Senateur, F. Weiss, A. Vantomme, G. Langouche, A.A. Melo, M.F. da Silva, J.C. Soares, J.B. Sousa and the ISOLDE collaboration, Nucl. Instrum. Methods B 147 (1998) 244.
[27] J.P. Araújo, J.G. Correia, U. Wahl, J.G. Marques, E. Alves, V.S. Amaral, A.A. Lourenço, V. Galindo, T. von Papen, J.P. Senateur, F. Weiss, A. Vantomme, G. Langouche, A.A. Melo, M.F. da Silva, J.C. Soares, J.B. Sousa and the ISOLDE collaboration, Nucl. Instrum. Methods B 148 (1999) 807.
[28] V.S. Amaral, J.G. Correia, A.A. Lourenço, J.G. Marques, J.A. Mendes, M.A. Baptista, J.P. Araújo, J.M. Moreira, J.B. Sousa, E. Alves, M.F. da Silva, J.C. Soares and the ISOLDE Collaboration, J. Magn. Magn. Mater. 177–181 (1998) 511.
[29] J.P. Araújo, U. Wahl, J.G. Correia, A.A. Lourenço, V. Galindo, J.P. Senateur, F. Weiss, A. Vantomme, G. Langouche, J.C. Soares, J.B. Sousa and the ISOLDE Collaboration, in preparation.